Pattern formation and phase transition in the collective dynamics of a binary mixture of polar self-propelled particles

Sagarika Adhikary and S. B. Santra
Department of Physics, Indian Institute of Technology Guwahati, Guwahati-781039, Assam, India

(Received 4 September 2021; revised 16 February 2022; accepted 24 May 2022; published 30 June 2022)

The collective behavior of a binary mixture of polar self-propelled particles (SPPs) with different motile properties is studied. The binary mixture consists of slow-moving SPPs (sSPPs) of fixed velocity v_s and fast-moving SPPs (fSPPs) of fixed velocity v_f. These SPPs interact via a short-range interaction irrespective of their types. They move following certain position and velocity update rules similar to the Vicsek model (VM) under the influence of an external noise η. The system is studied at different values of v_f keeping $v_s = 0.01$ constant for a fixed density $\rho = 0.5$. Different phase-separated collective patterns that appear in the system over a wide range of noise η are characterized. The fSPPs and the sSPPs are found to be orientationally phase synchronized at the steady state. We studied an orientational order-disorder transition varying the angular noise η and identified the critical noise η_c for different v_f. Interestingly, both the species exhibit continuous transition for $v_f < 100v_s$ and discontinuous transition for $v_f > 100v_s$. A new set of critical exponents is determined for the continuous transitions. However, the binary model is found to be nonuniversal as the values of the critical exponents depend on the velocity. The effect of interaction radius on the system behavior is also studied.

DOI: 10.1103/PhysRevE.105.064612

I. INTRODUCTION

Collective pattern formation and self-organization of active or self-propelled particles (SPPs) spontaneously occur in nature at different length scales. For example, actin filaments can form different structures as microclusters, stripes, and traveling waves [1,2], bacterial swarms growing in the laboratory can self-organize into high-density coherent patterns [3–7]; other examples include army ants [8], insect swarms [9,10], spiny lobsters [11,12], fish schools [13], flocking birds [14,15], pedestrian flow [16,17], and artificial systems of SPPs [18,19]. The collective behavior of polar SPPs is extensively studied following the seminal Vicsek model (VM) [20]. In this model, a large number of polar SPPs move together with equal speed v_0, and they align their direction of motion with their neighbors through a short-range (R) alignment interaction. However, the average direction is subject to an angular noise (η). For a given density (ρ_0), an orientational order-disorder transition occurs at a critical noise (η_c). Initially, the nature of this phase transition in the VM was found to be continuous for low velocity and small system sizes [21,22]. However, later it was established through extensive simulations that there exists a crossover system size $L^*(\rho_0, v_0)$ [23,24] below which the nature of the transition is continuous, and above which it is discontinuous where dense traveling bands appear in the system. It needs to be noted that $L^*(\rho_0, v_0)$ diverges both for low velocities ($v_0 < 0.05$) and low densities ($\rho_0 < 0.01$) [23]. The formation of the dense traveling band near the transition region is fluctuation driven and occurs due to the feedback mechanism between local order and local density [25].

One of the major limitations of the VM is that all the polar SPPs have the same motile property. For example, all the SPPs have the same velocity. However, in natural systems, the velocities of particles need not be the same during collective motion. For example, there are fast-moving (active) and slow-moving (dormant) bacteria in a bacterial population or slow-moving and speedy vehicles in daily traffic. Phase separation and static clusters were mainly observed in the study of collective dynamics of SPPs with variable speed (depending on the neighborhood's polarization) [26,27]. Apart from velocity, other properties of active particles are also varied to study the phase separation in different systems [28,29]. Examples of such systems include a mixture of active Brownian particles with different diffusion constant [30,31], a mixture of active and passive particles [32–35], binary active particles with different alignment interactions [36], an oppositely driven binary mixture of particles [37–39], chiral active matter [40,41], a mixture of polar and apolar SPPs [42], and many others.

However, the study of collective dynamics in a binary mixture of polar SPPs with different motile properties is a new area of research. This paper studies the collective dynamics of a mixture of two types of SPPs with widely different fixed velocities. The SPPs interact with local short-range interaction, and the dynamics evolve under an external noise. It is intriguing to observe whether self-organized pattern formation and phase separation occur in this binary model (BM) with a short-range interaction only. Furthermore, will there be any criticality in the system? Will the system undergo any order-disorder transition at a critical point? What would be the nature of such a transition? In this study, we explore answers to all these questions. The collective dynamics and the underlying mechanism could also explain the similar pattern formation and dynamical behavior observed in other systems.

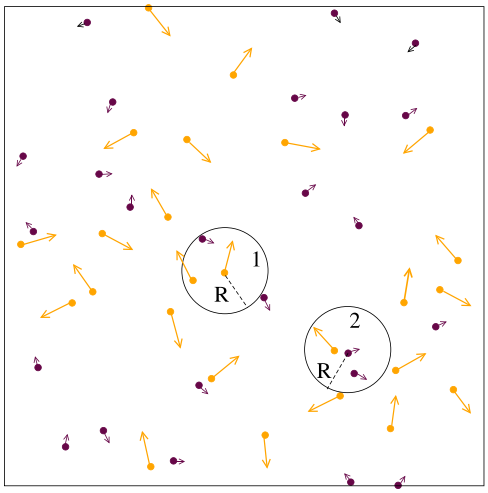

FIG. 1. The distribution of binary SPPs is shown on a system of size $L = 10$, where $N = \rho L^2 = 50$, $N_f = N_s = 25$. Orange and maroon colors represent fSPPs and sSPPs, respectively. The arrow associated with an SPP indicates the direction of velocity. A fSPP at the center of the circle-1 interacts with both the fSPP and sSPP present within the radius of R. Similarly, an sSPP at the center of the circle-2 interacts with both types of SPPs present within the radius R.

In the next section, we present the model and discuss the results obtained. Herein, polar SPPs will be referred to simply as SPPs.

II. MODEL

The collective motion of a mixture of SPPs with two different motilities is modeled over a two-dimensional square box of linear size L. The different motilities of SPPs are modeled, assigning widely different fixed velocities to them. The fast-moving SPPs (fSPPs) move with a velocity v_f and the slow-moving SPPs (sSPPs) move with a velocity v_s where $v_f \gg v_s$. The two types of SPPs are taken in equal proportion. If N_f is the number of fSPPs, and N_s is the number of sSPPs, then $N_f = N_s = N/2$ where N is the total number of SPPs in the system. Initially, the position $\vec{r}_{p,i}$, $i = 1, 2, 3, \ldots, N/2$ of all the SPPs are randomly distributed over the space (off lattice) where $p \in \{s, f\}$. The initial orientation θ_i of an SPP is randomly selected in the range $-\pi$ to π, irrespective of its type. The SPPs of both types interact within a local neighborhood $R = 1$ and determine their average orientation. There is no external force or interparticle repulsion. Both interparticle and intraparticle interactions are considered in estimating the average orientation. The distribution of 25 randomly oriented fSPPs (in orange) and 25 randomly oriented sSPPs (in maroon) is shown in Fig. 1. Longer and shorter arrows show the velocities v_f and v_s, respectively.

The time evolution of the orientation θ_i of the ith SPP is determined by

$$\theta_i(t + \Delta t) = \langle \theta(t) \rangle_R + \Delta\theta \tag{1}$$

where $\Delta\theta$ is a random orientation chosen with a uniform probability from the interval $[-\eta\pi, +\eta\pi]$. The strength of the angular noise η varies from 0 to 1. The term $\langle \cdots \rangle_R$ is defined as

$$\langle \theta(t) \rangle_R = \arctan\left[\frac{\langle \sin\theta \rangle}{\langle \cos\theta \rangle}\right],$$

$$\langle \sin\theta \rangle = \frac{1}{n}\sum_{j\in\{R\}} \sin\theta_j, \quad \langle \cos\theta \rangle = \frac{1}{n}\sum_{j\in\{R\}} \cos\theta_j,$$

where n is the number of SPPs in the neighborhood region R that includes both the sSPPs and fSPPs. It should be noted that the magnitude of velocity of individual SPPs are ignored and only the orientations are taken into account in estimating $\langle \theta(t) \rangle_R$. After averaging, an SPP of type p ($p \in \{s, f\}$) at the position $\vec{r}_{p,i}$ is thus moving with a speed v_p in the direction θ_i. Knowing the velocity $\vec{v}_{p,i}(t)$ at every time step, the position of the ith SPP $\vec{r}_{p,i}$ is updated following the forward update rule

$$\vec{r}_{p,i}(t + \Delta t) = \vec{r}_{p,i}(t) + \vec{v}_{p,i}(t)\Delta t, \tag{2}$$

where Δt is the time between two successive updates, and it is chosen as $\Delta t = 1$. Periodic boundary conditions (PBCs) in the horizontal and vertical directions are applied in case the position vector crosses the boundary of the square box. Equations (1) and (2) are then evolved with time and a steady state is achieved for a given noise η. The model is studied varying η over a wide range. The interaction considered in this model is purely aligning in nature and no steric or hydrodynamic interactions are present in the system. In the special situation where $v_s = v_f = v_0$, the BM is equivalent to the VM with velocity v_0 for all SPPs [20].

For a given initial random distribution of SPPs over a square box of size L, Monte Carlo simulations are performed to study the time evolution of the binary system following Eqs. (1) and (2). One Monte Carlo time step corresponds to incrementing the position and orientation of all the SPPs. The initial 7×10^5 Monte Carlo steps are neglected to achieve the steady state. An ensemble of size 48×10^5 is taken for statistical averages (2×10^5 samples at different times for 24 different initial configurations). Simulations are performed at different velocities: keeping $v_s = 0.01$ fixed, the value of v_f is taken as $v_f = 30v_s$, $v_f = 50v_s$, $v_f = 100v_s$, and $v_f = 150v_s$. The density of SPPs is kept fixed as $\rho = 0.5$ for all simulations. Thus, the total number of SPPs is $N = \rho L^2$. The numbers of sSPPs (N_s) and fSPPs (N_f) are taken in equal proportions, i.e., $N_f = N_s = N/2$.

III. COLLECTIVE PATTERNS AND THEIR CHARACTERIZATION

In this section, we will describe the morphological as well as structural changes of flocks of SPPs with noise. A flock is a collection of SPPs that are within the range of interaction R from each other. For this study, we consider the velocity of sSPPs as $v_s = 0.01$ and that of fSPPs as $v_f = 30v_s$. The morphology of the binary mixture at different noises is generated on a system of size $L = 128$ (total number of SPPs $N = 8192$, $N_f = N_s = 4096$). The morphology is shown in Fig. 2 where the orange color represents the fSPPs, and the maroon color represents the sSPPs. A variety of patterns of the flocks of sSPPs and fSPPs appear as the angular noise η varies.

For a low angular noise $\eta = 0.01$, the flocks of fSPPs are in the form of clusters and moving in a particular

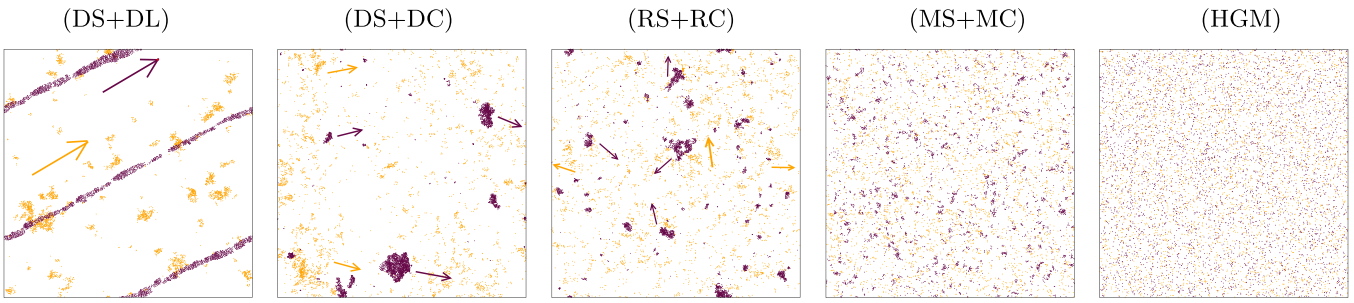

FIG. 2. System morphology with $v_f = 30v_s$ and $v_s = 0.01$ for different angular noise values (a) $\eta = 0.01$, (b) $\eta = 0.15$, (c) $\eta = 0.24$, (d) $\eta = 0.45$, and (e) $\eta = 0.70$ for a system of size $L = 128$, $N_f = N_s = 4096$. Orange: fSPPs; maroon: sSPPs.

direction (indicated by an orange arrow). On the other hand, the flocks of sSPPs form narrow lanes in the same direction (indicated by a maroon arrow) as that of fSPPs. The situation is shown in Fig. 2(a). It seems that in the binary system of SPPs, the dynamics of sSPPs is governed by the local shear between two SPPs. Since the sSPPs are slow movers, many fSPPs interact with them at a given time. Moreover, at each time step, the fSPPs travel a much larger distance than the sSPPs, and consequently they influence the ordering of the distant flocks of fSPPs as well as that of sSPPs. For a given initial configuration, the direction of motion of directed clusters (DSs) of fSPPs or directed lanes (DLs) of sSPPs, is spontaneously selected toward an arbitrary direction. Such lane formation was not observed in the VM with monodispersed SPPs. However, the formations of lanes and clumps were also observed in a model of SPPs with density-dependent motility [43]. Phase-separated bands of big and small particles oriented along the direction of the flow are also observed in a bidisperse granular system under shear flow [44].

As η is increased to 0.15, DSs of fSPPs look a little scattered, whereas the sSPPs form clumps (or compact clusters) that still move in the same direction as DSs as shown in Fig. 2(b). The orientation of the clumps of sSPPs remains synchronized with that of the DSs of fSPPs. We call these clumps of sSPPs directed clumps (DCs). Further increase of noise to $\eta = 0.24$ induces random motion to the flocks of both fSPPs and sSPPs, shown in Fig. 2(c). We call the randomly moving clusters of fSPPs random clusters (RSs) and the randomly moving clumps of the sSPPs random clumps (RCs). Thus, the orientationally ordered phase with DSs and DCs goes to an orientationally disordered phase with RSs and RCs as the noise changes from $\eta = 0.15$ to $\eta = 0.24$. The critical behavior of such a transition will be described in Sec. IV. As η is increased to 0.45, RSs and RCs are found to dissolve into a larger number of microclusters (MSs) of fSPPs and microclumps (MCs) of sSPPs, respectively, as shown in Fig. 2(d). For relatively high η, a homogeneous gaslike mixture (HGM) of both types of SPPs is observed, as shown in Fig. 2(e) for $\eta = 0.70$.

Similar patterns also appear in the cases of higher values of v_f, keeping $v_s = 0.01$. Now we characterize the patterns, considering a system of size $L = 256$ with $\rho = 0.5$. Thus, the total number of SPPs $N = 32\,768$, and the numbers of fSPPs and sSPPs are $N_f = N_s = 16384$.

A. Phase segregation

It is observed that the system remains phase separated over a wide range of noise η. The system is found to be phase separated, which means the sSPPs and fSPPs can be identified separately in space. A segregation coefficient [40,45] is defined as

$$S = \frac{1}{N}\sum_{j=1}^{Q} |n_f^{(j)} - n_s^{(j)}| \tag{3}$$

where $\sum_{j=1}^{Q}\{n_f^{(j)} + n_s^{(j)}\} = N$, the total number of SPPs, Q is the number of small square boxes of size $\ell \times \ell$ that cover the whole system of size $L \times L$, and n_f and n_s are the number of the fSPPs and sSPPs, respectively, in a small box. We have estimated S for a wide range of η, taking $\ell = 8$. Thus, $Q = L^2/\ell^2 = 1024$. As per Eq. (3), if every box is filled with either fSPPs or sSPPs (phase-separated), then $S = 1$, and if every box is filled with both fSPPs and sSPPs in equal proportion (homogeneous phase), then $S = 0$; whereas $S = 1/2$ corresponds to the situation that, on an average, $\Delta n = |n_f^{(j)} - n_s^{(j)}| \approx 16$ in every box. We consider the system to be phase separated if $S \geqslant 1/2$ and mixed if $S < 1/2$. The variation of S with η is shown in Fig. 3. It can be seen that the system remains phase separated up to a very high noise, $\eta \approx 0.36$. The value of S is greater than 0.8 for $\eta < 0.04$ at which the phase-separated DL and DS appear. The process

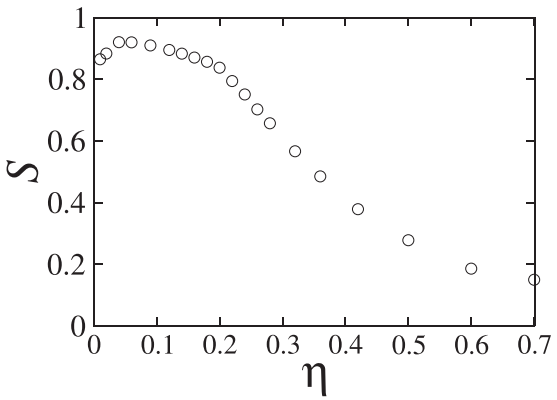

FIG. 3. $v_f = 30v_s$, $v_s = 0.01$: Plot of the segregation coefficient S versus η. System size is $L = 256$. The square box of area L^2 is divided into Q square subregions of linear size ℓ and area L^2/Q each.

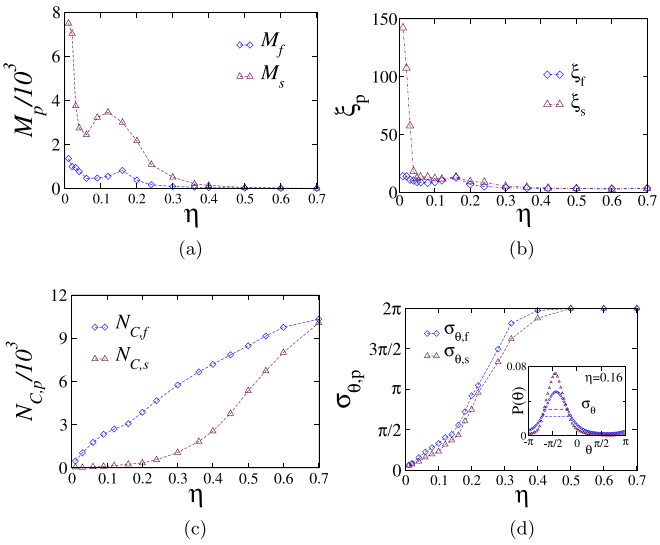

FIG. 4. $v_f = 30v_s$, $v_s = 0.01$: (a) Plot of M_p against η. (b) Plot of ξ_p against η. (c) Plot of $N_{C,p}$ against η. (d) Plot of $\sigma_{\theta,p}$ versus η. In the inset of (d), $P(\theta)$ is plotted for $\eta = 0.16$ with the same symbols and colors for the fSPPs and sSPPs. System size is $L = 256$.

of phase separation continues, and the system is found to be highly phase separated with $S \approx 0.9$ in the noise range $0.04 < \eta < 0.09$. Such a phase separation between the two species is due to the large velocity difference and the presence of noise in the system. For $\eta > 0.09$, S decreases monotonically with increasing η. This indicates a slow mixing of the two species of SPPs at high noise. Eventually, at $\eta \approx 0.70$, the phase separation disappears $S \approx 0.15$, and the two species of SPPs mix uniformly. Phase separation was also reported in a binary mixture of active Brownian particles with wide differences in the diffusion constant [30].

B. Characterization of patterns

To monitor the structural change in the patterns of the flocks, we have estimated the size (M_P) and extension (ξ_p) of the largest flock, and the number of flocks $N_{c,p}$ ($p \in \{s, f\}$) with noise η on a system of size $L = 256$. The largest flock size of p-type SPPs is given by the number of pSPPs that belong to the largest flock of that type, and the extension of a flock is just the gyration radius. To measure how the flocks of SPPs are ordered, we have estimated the full widths at half maxima σ_p of the orientation distribution $P(\theta)$, where σ_p can vary from 0 to 2π. Thus, σ_p represents the orderliness of the flocks: $\sigma_p = 0$ means they are highly ordered (moving in a particular direction) and $\sigma_p = 2\pi$ means they are completely disordered (moving in all possible directions). The variations of M_p, ξ_p, $N_{c,p}$, and σ_p against η are shown in Fig. 4.

For $\eta = 0.01$, the sSPPs have the largest flock of size $M_s \approx 8000$, extension $\xi_s \approx 150$ (half of the system size), and number of flocks $N_{c,s} \approx 50$; whereas the fSPPs have the largest flock of size $M_f \approx 1300$ (out of $N_f = 16384$), extension $\xi_f \approx 15$, and number of flocks $N_{c,f} \approx 500$. At this noise, the flock structure of sSPPs (DL) seems to be more compact in comparison to the DS of fSPPs. It should be noted that such a dense packing of slow-moving particles occurred in the absence of an attractive force. This has happened only due to the presence of small noise and high-velocity differences between the two types. The flocks are highly ordered, $\sigma_s = \sigma_f \approx \pi/15$.

As η is increased to 0.06, a drastic change happens to the flock structure of sSPPs. The largest flock size of sSPPs is $M_s \approx 2500$, the extension is $\xi_s \approx 12$, and the number of flocks is $N_{c,s} \approx 70$. For fSPPs, the largest flock size is $M_f \approx 500$, the extension is $\xi_f \approx 10$, and number of flocks is $N_{c,f} \approx 1700$. The change in the structure of sSPPs is remarkable in comparison to that of fSPPs. It seems there is a noise-induced melting transition happening in the system. However, it needs to be characterized carefully with further studies. The orderliness of the flocks is $\sigma_s = \sigma_f \approx \pi/6$.

On further increase of η to 0.12–0.16, both sSPPs and fSPPs rebuild their largest flocks. For sSPPs at $\eta = 0.12$, the largest flock size is $M_s \approx 3400$ and the extension is $\xi_s \approx 12$. The number of flocks has increased to $N_{c,s} \approx 160$. The orderliness $\sigma_s \approx \pi/3$. For fSPPs at $\eta = 0.16$, the largest flock size is $M_f \approx 800$ and the extension is $\xi_f \approx 12$. The number of flocks has increased to $N_{c,f} \approx 3000$. The orderliness $\sigma_f \approx \pi/2$. In the intermediate range of η, it is observed that $\sigma_f > \sigma_s$. Once again it should be noted that the aggregation of flocks is happening in the absence of any attractive force. The orientation distributions $P(\theta)$ for both the SPPs are given in the inset of Fig. 4(d) for $\eta = 0.16$.

The above properties are found to decrease monotonically with increasing η beyond 0.16. These parameters remain ineffective in determining the orientational order-disorder transition that occur at $\eta \approx 0.19$. However, near the transition point ($\eta = 0.20$) the largest flock sizes are $M_s \approx 2000$, $M_f \approx 400$ and the extensions are $\xi_s \approx 9$, $\xi_f \approx 7$. The number of flocks are $N_{c,s} \approx 350$, $N_{c,f} \approx 4000$. Both the orderliness values σ_s and σ_f are close to π. In the high noise limit ($0.40 \leqslant \eta \leqslant 0.70$), both sSPPs and fSPPs have similar properties such as largest flock sizes are $M_s = M_f \approx 60$, extensions are $\xi_s = \xi_f \approx 4$. The number of flocks are $N_{c,s} = N_{c,f} \approx 10000$ when total numbers sSPPs and fSPPs are $N_f = N_s = 16384$. The orderliness of both the species is the lowest, $\sigma_f = \sigma_s = 2\pi$.

C. Velocity correlations

The spatial correlation is measured by the two-point velocity correlation function $g(r)$ and the temporal correlation is measured by the velocity time autocorrelation function $C(t)$. Following Ref. [46], they are given by

$$g(r) = \left\langle \frac{\vec{v}_i(0) \cdot \vec{v}_j(r)}{|\vec{v}_i(0)||\vec{v}_j(r)|} \right\rangle, \quad C(t) = \left\langle \frac{\vec{v}_i(0) \cdot \vec{v}_i(t)}{|\vec{v}_i(0)||\vec{v}_i(t)|} \right\rangle, \qquad (4)$$

where i and j are particle indices, t is the time interval, r is distance between i and j, and $\langle \cdots \rangle$ stands for an ensemble average over $1000 \times N$ configurations. The values of $g(r)$ versus r and $C(t)$ versus t are estimated for three different noise values around the critical point as $\eta = 0.15$, $0.19(\eta_c)$, and 0.24. The $g(r)$ and $C(t)$ values are plotted in Figs. 5(a) and 5(b) against r and t respectively in semilogarithmic scale. The critical correlations $g(r)$ or $C(t)$ at $\eta_c = 0.19$ curves are in red, the brown curves represent the $g(r)$ or $C(t)$ in the ordered (DS+DC) phase, and the green curves represent the $g(r)$ or $C(t)$ in the disordered (RS+RC) phase.

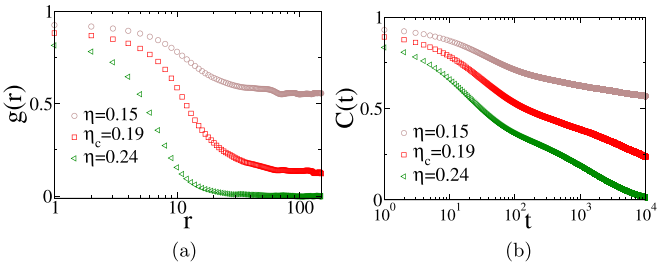

FIG. 5. $v_f = 30v_s$, $v_s = 0.01$: (a) Plot of $g(r)$ against r. (b) Plot of $C(t)$ against t. System size is $L = 256$.

It can be seen from Fig. 5(a) that the correlation $g(r)$ decays faster for $r > 10$. In this region, the extension of the flocks (ξ_p) is found to be of the order of ξ_f, $\xi_s \approx 10$. As a result, the velocity orientation is correlated among the SPPs present in the same flock, and the correlation is found to be strong for $r < 10$. In the subcritical regime ($\eta < 0.19$, shown in brown), a strong correlation [$g(r) > 0.5$] is sustained all over the system. In the upper critical regime ($\eta > 0.19$, shown in green), the correlation decays very fast and goes to zero at $r \approx 50$. However, the critical correlation $g(r)$ ($\eta_c = 0.19$) is sustained with a smaller value [$g(r) \approx 0.15$] up to a distance of the order of system size. It is expected that, at the criticality, the correlation length should be of the order of system size. With a small increase in noise, such correlation could be destroyed, as seen in the case of $\eta = 0.24$, and, on reducing the noise, $g(r)$ increases as seen in the case of $\eta = 0.15$. It is important to notice that even though the interaction is short ranged, the correlation extends up to system size.

It can be seen in Fig. 5(b) that the autocorrelation $C(t)$ is very high over a long time t, irrespective of η. The critical $C(t)$ is sustained for a long time $t > 10^4$. The $C(t)$ at η_c is always less than $C(t)$ for the DS+DC phase, and it is always greater than $C(t)$ for the RS+RC as expected. The $C(t)$ for $\eta = 0.24$ goes to zero at $t = 10^4$ whereas for $\eta = 0.15$ it is $\approx$0.56 at $t = 10^4$ and continues to be high beyond this t. It seems that once dense flocks are formed in the system, they stay for a long time, and a strong correlation exists in the ordered phase, whereas the flocks in the disordered phase seem to be less stable due to the randomness among the SPPs.

IV. PHASE TRANSITION

As the angular noise η varies, the system undergoes a transition from an orientational ordered state to an orientational disordered state. In this model, such a transition occurs when the DS+DC phase [Fig. 2(b)] changes to the RS+RC phase [Fig. 2(c)] around the critical noise $\eta = \eta_c$. The order parameter of the transition is defined as

$$\phi(\eta, L) = \sum_{p=f,s} \phi_p(\eta, L), \quad \phi_p(\eta, L) = \frac{1}{N_p}\left|\sum_{i=1}^{N_p} \frac{\vec{v}_{p,i}}{|\vec{v}_{p,i}|}\right|, \quad (5)$$

where ϕ represents the total order parameter, ϕ_p ($p \in \{s, f\}$) is the partial order parameter, and N_p is the number of p-type SPPs. The susceptibility χ for the whole system and that of the partial systems χ_p can be estimated from the fluctuation in their respective order parameters ϕ and ϕ_p as

$$\chi = L^2[\langle\phi^2\rangle - \langle\phi\rangle^2], \quad \chi_p = L^2\left[\langle\phi_p^2\rangle - \langle\phi_p\rangle^2\right], \quad (6)$$

where $\langle\phi^n\rangle = \int \phi^n P(\phi) d\phi$, $\langle\phi_p^n\rangle = \int \phi_p^n P(\phi_p) d\phi_p$, and $P(\phi)$ and $P(\phi_p)$ are the distribution functions of ϕ and ϕ_p respectively. Similarly, the fourth-order Binder cumulant for the whole system and that of the partial systems are defined as

$$U = 1 - \frac{\langle\phi^4\rangle}{3\langle\phi^2\rangle^2}, \quad U_p = 1 - \frac{\langle\phi_p^4\rangle}{3\langle\phi_p^2\rangle^2}, \quad (7)$$

where the higher order averages are obtained following the definitions of $\langle\phi^n\rangle$ and $\langle\phi_p^n\rangle$ given above.

If the orientational order-disorder transition is continuous, the finite size scaling (FSS) relations of the above parameters can be given following the equilibrium thermal critical phenomena [47,48], as

$$\phi(\eta, L) = L^{-\beta/\nu}\phi_0[\epsilon L^{1/\nu}], \quad (8)$$

where $\epsilon = (\eta - \eta_c)/\eta_c$ the reduced noise, β is the order parameter exponent, ν is the correlation length exponent, and ϕ_0 is a scaling function. At the criticality $\eta = \eta_c$, $\phi(\eta_c, L) \sim L^{-\beta/\nu}$. The order parameter distribution $P_L(\phi)$ for a given system of size L is defined as

$$P_L(\phi) = L^{\beta/\nu}\widetilde{P}_L[\phi L^{\beta/\nu}], \quad (9)$$

where $\widetilde{P}_L$ is a scaling function. At the criticality, the distribution $P_L(\phi)$ is unimodal for a continuous transition. The FSS form of the susceptibility is given by

$$\chi(\eta, L) = L^{\gamma/\nu}\chi_0[\epsilon L^{1/\nu}], \quad (10)$$

where χ_0 is a scaling function, $\gamma/\nu = d - 2\beta/\nu$, and d (= 2) is the number of space dimensions. At $\eta = \eta_c$, $\chi(\eta_c, L) \sim L^{\gamma/\nu}$. The FSS form of the fourth-order Binder cumulant is given by

$$U(\eta, L) = U_0[\epsilon L^{1/\nu}], \quad (11)$$

where U_0 is a scaling function. The derivative of $U(\eta, L)$ with respect to η follows a scaling relation [49],

$$U'(\eta, L) = L^{1/\nu}\frac{U_0'[\epsilon L^{1/\nu}]}{\eta_c}, \quad (12)$$

where the primes on U and U_0 denote their derivatives with respect to η. For a continuous transition, the cumulant U always remain positive. At $\eta = \eta_c$, the cumulants of different systems of size (L) become independent of L and $U'(\eta_c, L) \sim L^{1/\nu}$ at the transition.

In the case where the orientational order-disorder transition is discontinuous, the order parameter exponent β should go to zero. As a consequence, the susceptibility should then scale as $\chi \sim L^d$, where d is the space dimension. The Binder cumulant U would exhibit a sharp fall towards a negative value at the transition point. As the system exhibits the coexistence of two phases, the order parameter distribution $P(\phi)$ would be a bimodal distribution.

Below we discuss results of three different velocity scenarios. Keeping $v_s = 0.01$ fixed, $v_f = 30v_s$, $v_f = 50v_s$, and $v_f = 150v_s$ are taken. In all three scenarios, we study variations of order parameter ϕ, Binder cumulant U, susceptibility

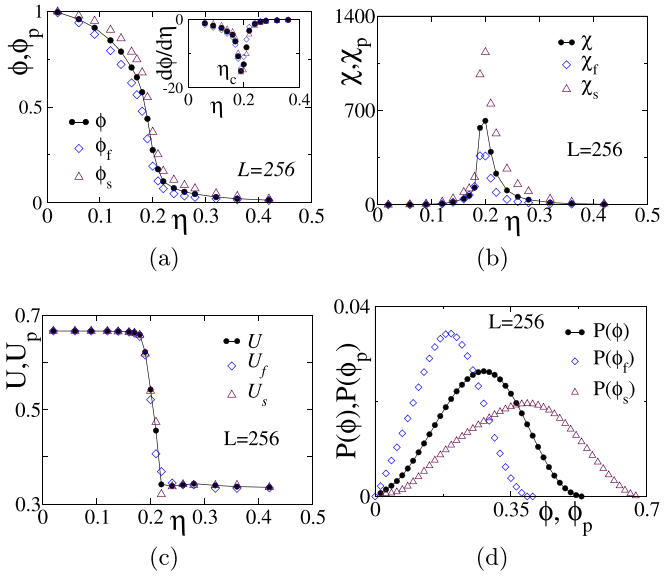

FIG. 6. $v_f = 30v_s$, $v_s = 0.01$: (a) Plot of ϕ and ϕ_p vs η. Derivatives of ϕ and ϕ_p with respect to η are shown in the inset. (b) Plot of χ and χ_p vs η. (c) Plot of U and U_p vs η. (d) Plot of $P(\phi)$ and $P(\phi_p)$ at $\eta = \eta_c$. System size is $L = 256$.

χ, and order parameter distribution $P(\phi)$ as a function of the angular noise η on systems of different sizes L, and we discuss the results together in the Discussion section.

A. Velocities: $v_f = 30v_s$ and $v_s = 0.01$

In Fig. 6, we present data for ϕ, U, χ, and $P(\phi)$ for $v_f = 30v_s$ on a system of size $L = 256$. The values of ϕ and ϕ_p decrease continuously and smoothly from a positive value to zero as η increases. The derivatives of ϕ and ϕ_p with respect to η are plotted in the inset of Fig. 6(a). A minimum or dip at $\eta \approx 0.19$ is observed in the derivatives. This is the critical noise $\eta_c = 0.19$ at which the systems undergo a phase transition. It is evident from the configurations given in Figs. 2(b) and 2(c) that the system is going from an ordered phase DS+DC to a disordered phase RS+RC around $\eta_c \approx 0.19$. The fluctuations in order parameters χ and χ_p are plotted against η in Fig. 6(b) for $L = 256$. All the fluctuations diverge at $\eta_c \approx 0.19$. The order parameter fluctuation of the sSPPs at η_c is much higher than that of the fSPPs. It is similar to the observations in the VM with monodispersed SPPs. The Binder cumulants U and U_p are plotted against η in Fig. 6(c) for $L = 256$. It can be seen that the values of U, U_f, and U_s are all positive over the whole range of η. The distributions of order parameters $P(\phi)$ and $P(\phi_p)$ obtained at $\eta = \eta_c$ are presented in Fig. 6(d). All three distributions are found to be unimodal. The positive value of the Binder cumulant and unimodal distribution of ϕ indicates a continuous transition.

The critical exponents are extracted for the whole system with $v_f = 30v_s$ by performing FSS analysis. Binder cumulant U, order parameter ϕ, and susceptibility χ are plotted against the angular noise η for three different systems of sizes $L = 64$, 128, and 256 in Figs. 7(a), 7(b), and 7(c) respectively. The plots of U versus η [Fig. 7(a)] for different L intersect at $\eta_c \approx 0.19$, the L independent critical point, as expected in a continuous transition. It is marked by a cross on the η axis. The corresponding U_c is identified as $U_c \approx 0.61$, which is close to that of a mono-dispersed system [50]. Rough estimates of the exponents $1/\nu$, β/ν, and γ/ν are obtained from the scaling relations $U'(\eta_c, L) \sim L^{1/\nu}$, $\phi(\eta_c, L) \sim L^{-\beta/\nu}$, and $\chi(\eta_c, L) \sim L^{\gamma/\nu}$ at the criticality. The best possible FSS forms of the scaled parameters against the scaled noise $\epsilon L^{1/\nu}$ are obtained, tuning these exponents further. U, $\phi L^{\beta/\nu}$, and $\chi L^{-\gamma/\nu}$

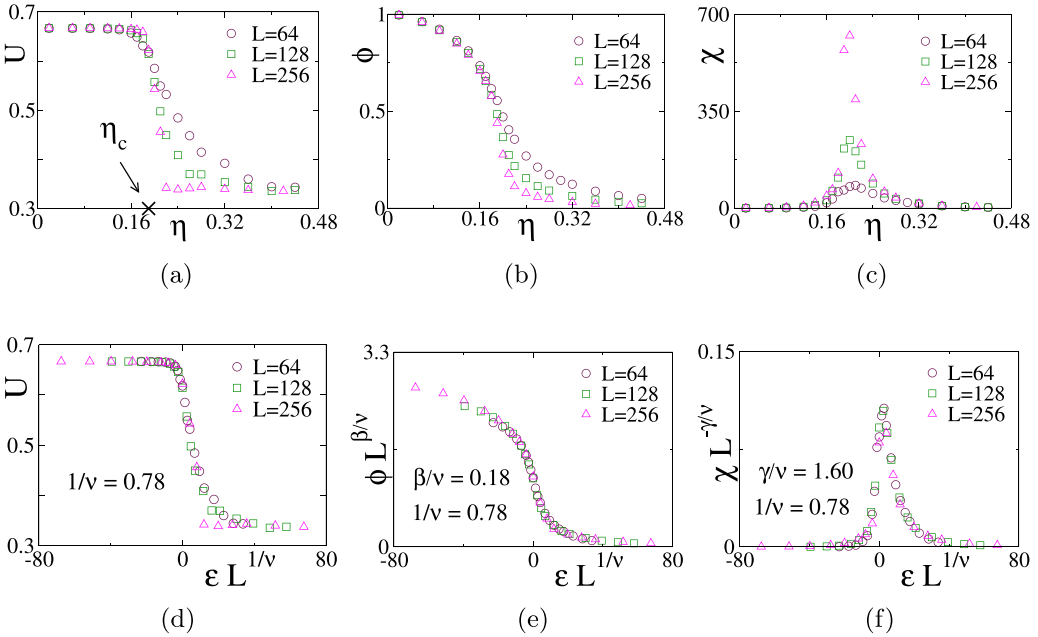

FIG. 7. $v_f = 30v_s$, $v_s = 0.01$: (a) Plot of U vs η, (b) plot of ϕ vs η, and (c) plot of χ vs η for $L = 64$, 128, and 256. The cross on the η axis indicates η_c. (d) Plot of U vs the scaled noise $\epsilon L^{1/\nu}$. (e) Plot of $\phi L^{\beta/\nu}$ against $\epsilon L^{1/\nu}$. (f) Plot of $\chi L^{-\gamma/\nu}$ against $\epsilon L^{1/\nu}$. The values of the exponents are taken as $\beta/\nu = 0.18$, $\gamma/\nu = 1.60$, and $1/\nu = 0.78$.

TABLE I. Values of the critical exponents obtained for the BM at different velocities of fSPPs $v_f = 30v_s$ and $50v_s$ keeping $v_s = 0.01$. The exponents for the VM with $v_0 = 0.1$ and density $\rho = 1/8$ to $3/4$ (taken from Ref. [50]) are presented for comparison.

Exponent	VM $v_0 = 0.1$	BM: $v_f = 30v_s$, $v_s = 0.01$	BM: $v_f = 50v_s$, $v_s = 0.01$
$1/\nu$	0.62(12)	0.78(9)	1.01(5)
β/ν	0.275(5)	0.18(1)	0.18(2)
γ/ν	1.45(2)	1.60(4)	1.60(8)
$\gamma/\nu + 2\beta/\nu$	2.00(3)	1.96(4)	1.96(8)

are plotted against $\epsilon L^{1/\nu}$ in Figs. 7(d), 7(e), and 7(f) respectively. A reasonable collapse of data in all three cases is obtained taking $1/\nu = 0.78$, $\beta/\nu = 0.18$, and $\gamma/\nu = 1.60$ at $\eta_c = 0.19$. The critical exponents satisfy the scaling relation $\gamma/\nu + 2\beta/\nu = 2$ within error bars. The values of these critical exponents are reported in Table. I. The FSS forms of U_p, ϕ_p, and χ_p for the partial systems are also verified, and the scaling relations are satisfied with the same critical exponents within error bars.

B. Velocities: $v_f = 50v_s$ and $v_s = 0.01$

The order parameters ϕ and ϕ_p are plotted against η in Fig. 8(a). The values of ϕ and ϕ_p decrease smoothly to zero as η increases. The derivatives of ϕ and ϕ_p with respect to η are plotted in the inset of Fig. 8(a) and minima of the plots at the transition noise $\eta_c \approx 0.22$ are observed. ϕ_f is also less than ϕ_s as in the $v_f = 30v_s$ situation. The respective fluctuations in order parameter, χ, and χ_p are plotted against η in Fig. 8(b). They diverge at $\eta_c \approx 0.22$ for all the SPPs. The morphology of the system around the transition point is presented in Fig. 8. The phase transition occurs at $\eta_c \approx 0.22$ between the DS+DC phase and the RS+RC phase. The DS+DC phase at $\eta = 0.18$ is shown in Fig. 8(c) and the RS+RC phase at $\eta = 0.26$ is shown in Fig. 8(d). The arrows indicate the directions of motion of the clusters and clumps of different phases. It can be noticed that all the clusters and clumps in DS+DC are moving in a similar direction, whereas they are random in RS+RC.

In Fig. 8(e), U and U_p are plotted against η. Both U and U_p remain positive over the whole range of η. In Fig. 8(f), the distributions of order parameters $P(\phi)$ and $P(\phi_p)$ are plotted at $\eta = \eta_c$. The distributions are unimodal. The positive Binder cumulants and unimodal distributions of order parameters indicate a continuous transition in the whole system as well as in the partial systems for the case of $v_f = 50v_s$.

Since the transitions are continuous, we perform the FSS analysis to extract the critical exponents. The values of U, ϕ, and χ are plotted against η in Figs. 9(a), 9(b), and 9(c) respectively for different system sizes $L = 64$, 128, and 256. The plots of U versus η in Fig. 9(a) for different L intersect at $\eta_c \approx 0.22$, marked by a cross on the η axis. The corresponding critical value of the cumulant is $U_c \approx 0.61$. It seems the value of U_c is independent of the velocity ratio in this model. As in the case of $v_f = 30v_s$, rough estimates of the exponents $1/\nu$, β/ν, and γ/ν are obtained from the critical scaling relations $U'(\eta_c, L) \sim L^{1/\nu}$, $\phi(\eta_c, L) \sim L^{-\beta/\nu}$, and $\chi(\eta_c, L) \sim L^{\gamma/\nu}$. The best possible FSS forms of the scaled parameters

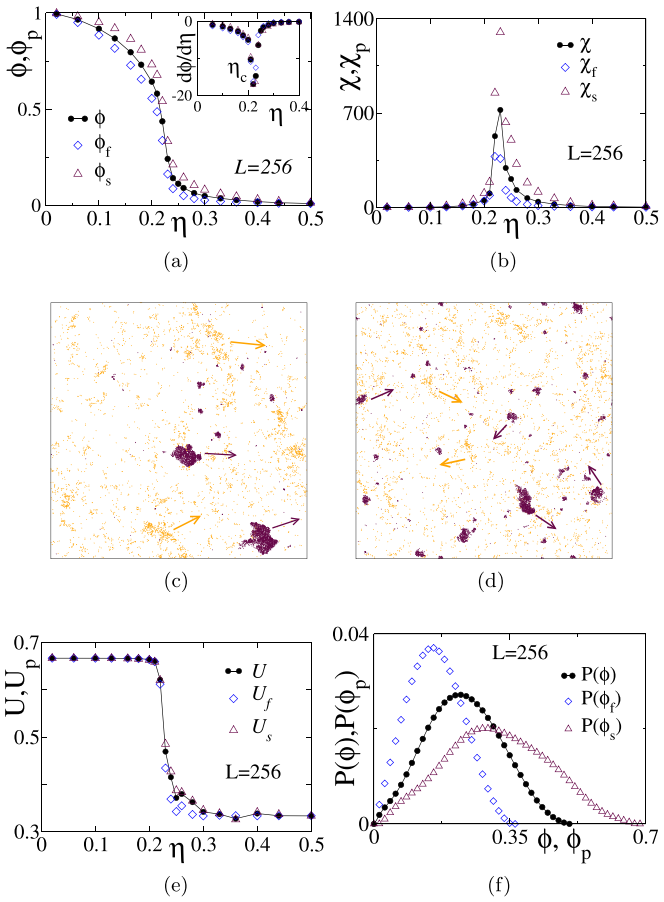

FIG. 8. $v_f = 50v_s$, $v_s = 0.01$: (a) Plot of ϕ and ϕ_p vs η. Derivatives of ϕ and ϕ_p with respect to η are shown in the inset. (b) Plot of χ and χ_p vs η. System size is $L = 256$. (c) Morphology of the system for $L = 128$ and $\eta = 0.18$; (d) for $\eta = 0.26$. Orange: fSPPS; maroon: sSPPs. The arrows represent the directions of motion. (e) Plot of U and U_p versvsus η. (f) Plot of $P(\phi)$ and $P(\phi_p)$ at η_c. System size is $L = 256$.

against the scaled noise $\epsilon L^{1/\nu}$ are obtained tuning these exponents further. The values of U, the scaled order parameter $\phi L^{\beta/\nu}$, and the scaled susceptibility $\chi L^{-\gamma/\nu}$ are plotted against $\epsilon L^{1/\nu}$ in Figs. 9(d), 9(e), and 9(f) respectively. A reasonable collapse of data in all three cases is obtained tuning the exponents further to $1/\nu = 1.01$, $\beta/\nu = 0.18$, and $\gamma/\nu = 1.60$. The exponents satisfy the scaling relation $\gamma/\nu + 2\beta/\nu = 2$ within error bars. The values of the critical exponents obtained are also given in Table I and compared with others.

C. Velocities: $v_f = 150v_s$ and $v_s = 0.01$

We now present simulation results obtained for $v_f = 150v_s$ keeping $v_s = 0.01$. The order parameters ϕ and ϕ_p are plotted against η in Fig. 10(a). There are jumps in the values of ϕ and ϕ_p near the transition. The derivatives of ϕ and ϕ_p with respect to η are plotted in the inset of Fig. 10(a) and sharp minima are observed at $\eta_c \approx 0.33$ for the whole and the partial systems. The respective fluctuations in order parameters, χ and χ_p, are plotted against η in Fig. 10(b). There is a sharp peak in the fluctuations at $\eta_c \approx 0.33$ for all the SPPs. In the inset of Fig. 10(b), the scaled fluctuations χ/L^2 are plotted

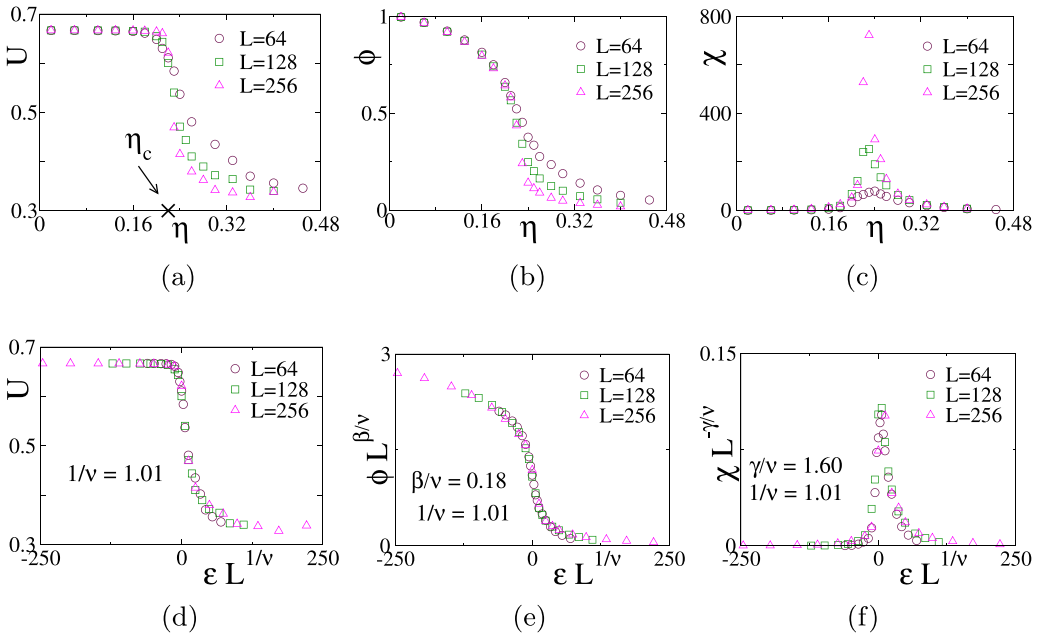

FIG. 9. $v_f = 50v_s$, $v_s = 0.01$: (a) Plot of U vs η, (b) plot of ϕ vs η, and (c) plot of χ vs η for $L = 64$, 128, and 256. The cross on the η axis indicates η_c. (d) Plot of U vs the scaled noise $\epsilon L^{1/\nu}$. (e) Plot of $\phi L^{\beta/\nu}$ against $\epsilon L^{1/\nu}$. (f) Plot of $\chi L^{-\gamma/\nu}$ against $\epsilon L^{1/\nu}$. The values of the exponents are taken as $\beta/\nu = 0.18$, $\gamma/\nu = 1.60$, and $1/\nu = 1.01$.

against ϵ for different systems of sizes $L = 64$, 128, and 256. The critical values (peak values) of scaled χ become almost L independent. Hence, $\chi \sim L^2$, as in the case of a discontinuous transition.

Plots of the Binder cumulants U and U_p versus η are shown in Fig. 10(c). The cumulant for the fSPPs, U_f, and that of the whole system, U, have sharp negative dips at the transition. However, the cumulant of the sSPPs (U_s) has

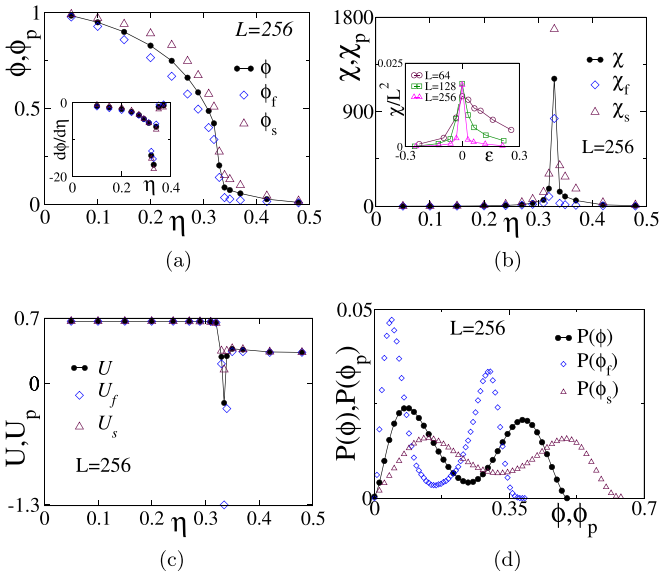

FIG. 10. $v_f = 150v_s$, $v_s = 0.01$: (a) Plot of ϕ and ϕ_p vs η. Derivatives of ϕ and ϕ_p with respect to η are shown in the inset. (b) Plot of χ and χ_p vesrsus η. In the inset, χL^{-2} is plotted against ϵ for $L = 64$, $L = 128$, and $L = 256$. (c) Plot of U and U_p vs η. (d) Plot of $P(\phi)$ and $P(\phi_p)$ at η_c.

a dip at the transition, but it has yet to achieve a negative value. The distributions of order parameters $P(\phi)$ and $P(\phi_p)$ at $\eta = \eta_c$ are shown in Fig. 10(d). For this high velocity, all three distributions exhibit bimodal distributions. These are characteristic features of a discontinuous transition. Since discontinuous transition is known to occur at high velocities in the monodispersed SPPs [23], it is expected to occur in the case of fSPPs, but it is surprising that the sSPPs are also undergoing discontinuous transition, which is unusual for sSPPs with such a low velocity $v_s = 0.01$. At the transition, dense traveling bands of SPPs form and disappear, resulting in coexistence of two phases in the system. It is then important to verify whether or not this is the case for the fSPPs here. More interestingly, what will the two phases be for the sSPPs? Below we explain the situation by studying the time evolution of the system morphology at the transition region.

The morphologies of a system of size $L = 256$ at two different time instants 3×10^5 and 4×10^5 are shown in Figs. 11(a) and 11(b) respectively for $\eta = \eta_c$. In Fig. 11(a), a dense traveling band of fSPPs and clumps of sSPPs are seen. Interestingly, the band and clumps are moving in the same direction, as indicated by the orange and maroon arrows, respectively. However, in Fig. 11(b), the dense traveling band of fSPPs disappears, and the clumps of sSPPs move randomly in the system. The orientation distributions $P(\theta)$ corresponding to phases (a) and (b) are shown in Fig. 11(c)-I and -II respectively. In Fig. 11(c)-I, $P(\theta)$ of both the SPPs are peaked at a particular θ. Thus, the sSPPs follow the direction of motion of the dense band of the fSPPs. As a band forms, the majority of the fSPPs travel in a particular direction. These highly oriented fSPPs interact with the sSPPs and influence them to orient in the same direction, whereas in Fig. 11(c)-II the distributions $P(\theta)$ for both the SPPs are flat. Hence, as the

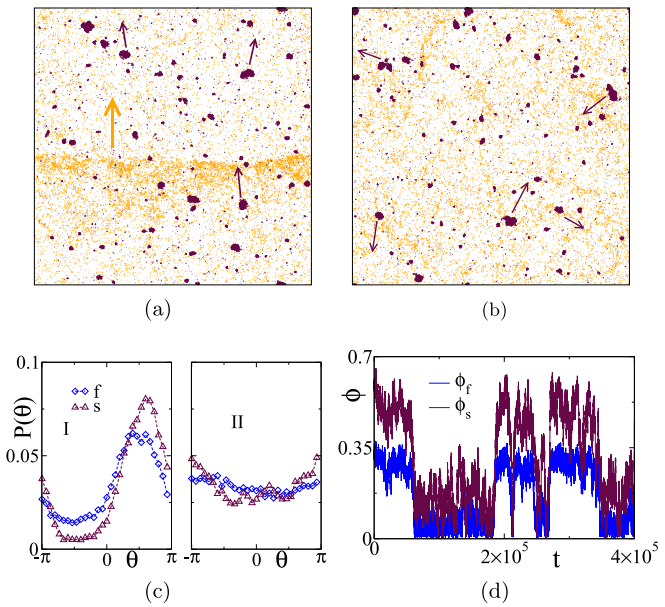

FIG. 11. $v_f = 150v_s$, $v_s = 0.01$: Morphology at (a) $t = 3\times10^5$ and (b) $t = 4\times10^5$ for $\eta_c = 0.33$ on a system of size $L = 256$. Orange: fSPPs; maroon: sSPPs. (c) $P(\theta)$ of the morphology (a) and (b) are plotted in I and II. (d) Order-parameter dynamics at η_c.

band disappears, the fSPPs get oriented randomly, making the orientation of sSPPs random.

The steady-state dynamics at $\eta = \eta_c$ of ϕ_f and ϕ_s are given in Fig. 11(d) where the values of both ϕ_f (blue) and ϕ_s (maroon) oscillate between two phases in a synchronized manner. The higher value of ϕ_f corresponds to the presence of the dense band (an ordered phase), and the lower value of ϕ_f corresponds to the disappearance of the band (a random or disordered phase). On the other hand, for the sSPPs, the higher value of ϕ_s corresponds to the ordered phase of directed clumps (DC) without forming any traveling band, and the lower value of ϕ_s corresponds to a disordered phase of random clumps (RC).

D. Discussion

In this binary model, an orientational order-disorder phase transition is found to occur at the respective η_c for different velocity cases, and the transition nature is also characterized. For both the $v_f = 30v_s$ and $v_f = 50v_s$ cases, a continuous transition occurs in the system from the DS+DC phase to the RS+RC phase. However, this is quite surprising for the fSPPs, with the velocity $v_f = 50v_s = 0.5$. For the velocity $v_0 = 0.5$ and density $\rho_0 = 0.25$, it is known that the crossover system size $L^*(\rho_0, v_0) \approx 150$ [23] to observe discontinuous transition in the VM. However, in the BM, no density bands of fSPPs with $v_f = 50v_s$ occur when mixed with the sSPPs ($v_s = 0.01$) even at a system size $L = 256$ much higher than the crossover size L^*. It seems that sSPPs have a significant influence on the nonformation of traveling bands by the fSPPs as well as on the nature of the phase transition. It is interesting to observe that both types of SPPs maintain the same nature of transition in the BM. Though the nature of transition with $v_f = 30v_s$ and $v_f = 50v_s$ remains the same as the VM at low velocities, the values of the critical exponents, however, are different (shown in Table I). Not only are the exponents different from those in VM, but they are also velocity dependent. Hence, the binary model is nonuniversal.

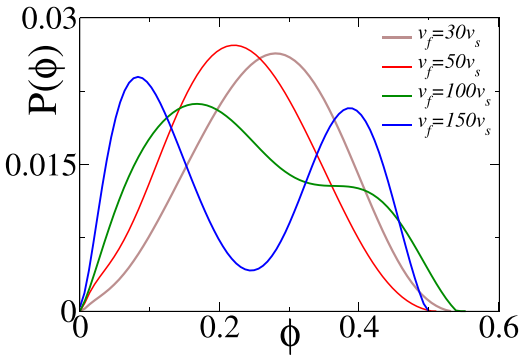

FIG. 12. Plot of $P(\phi)$ at the respective η_c's for different values of v_f as $30v_s$, $50v_s$, $100v_s$, and $150v_s$ with fixed $v_s = 0.01$. The system size is $L = 256$.

The $v_f = 150v_s$ case is very different from the previous two scenarios. In this case, the discontinuous transition was observed for both fSPPs and sSPPs because of phase synchronization. Such a phase synchronization occurs because of the local alignment [Eq. (1)]. Though the sSPPs show a discontinuous transition, they do not form any traveling density band in the system. Thus, the two different species are not able to undergo two different types of transitions, continuous or discontinuous, simultaneously in the BM because of the local interparticle interaction.

A crossover from continuous to discontinuous transition is expected at an intermediate v_f. This could be identified by plotting the order parameter distribution $P(\phi)$. The distribution will be unimodal for continuous transition and bimodal for discontinuous transition. In Fig. 12, $P(\phi)$ is plotted for different v_f's. It starts deviating from the unimodal distribution near $v_f = 100v_s$. It is important to note that this crossover value of v_f is determined for the fixed system of size $L = 256$ and density $\rho = 0.5$.

V. EFFECT OF INTERACTION RADIUS *R*

The value of R essentially determines the number of neighbors (n) to interact for an SPP at every move. So n decreases as R decreases. So far, the interaction radius R for both the SPPs was set to 1. It is important to know the effect of interaction radius R on the system with high velocity ratio $v_f = 150v_s$ among two SPPs. First, we investigate reducing the interaction radius to $R = 0.25$ for both the SPPs. The order parameters (ϕ and ϕ_p) and the Binder cumulants (U and U_p) are plotted against η in Figs. 13(a) and 13(b) respectively. It can be seen that all the order parameters continuously go to zero at a critical noise $\eta_c \approx 0.11$, which is much less than the $\eta_c = 0.33$ with $R = 1$. Such a behavior is also observed in the monodispersed case [49]. Moreover, U, U_f, and U_s are all found to be positive. In the inset of Fig. 13(b), $P(\phi)$ and $P(\phi_p)$ are plotted at η_c and all three distributions are unimodal. Thus the discontinuous transition for $R = 1$ becomes continuous for $R = 0.25$ for both the SPPs with $v_f = 150v_s$, $v_s = 0.01$.

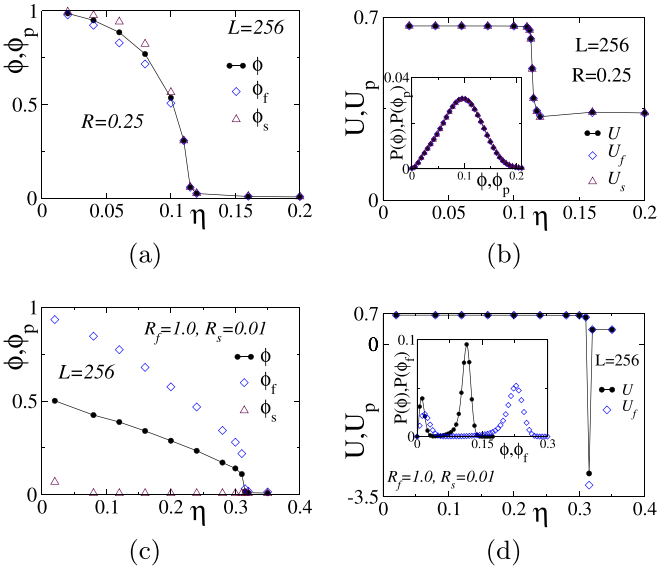

FIG. 13. $v_f = 150v_s$, $v_s = 0.01$: Plots of (a) ϕ and ϕ_p and (b) U and U_p vs η for $R = 0.25$. In the inset of (b), $P(\phi)$ and $P(\phi_p)$ at η_c are plotted. Plots of (c) ϕ and ϕ_p and (d) U and U_f vs η for $R_f = 1.0$ and $R_s = 0.01$. In the inset of (d), $P(\phi)$ and $P(\phi_f)$ at η_c are plotted. System size is $L = 256$.

Because of the reduced interaction region, very few SPPs participate in providing the average orientation to a particular SPP, so the coupling among the SPPs becomes weak. It has two effects. First, because of the weak coupling, the transition occurs at a lower value of η ($\approx$0.11). Second, the fSPPs are also not able to bind the other fSPPs to form a dense band at the transition point.

As a second case, we study the same system with different interaction radii for two types of SPPs. Two different radii are taken as $R_f = 1.0$ and $R_s = 0.01$ for the fSPPs and sSPPs respectively. The order parameter ϕ and ϕ_p are plotted against η in Fig. 13(c). Note that $\phi_s \approx 0$ for the whole range of η, because the interaction radius is so small that the sSPPs have almost no other particles to interact with, for this ρ. On the other hand the fSPPs having $R_f = 1$ undergo a discontinuous transition at $\eta_c \approx 0.32$, slightly less than the case with $R_f = R_s = 1$ and $v_f = 150v_s$, $v_s = 0.01$. In the present scenario, the sSPPs are noninteracting particles, and the fSPPs are the only active and interacting particles in the system. The system behavior is governed by the fSPPs only. The discontinuous transition is then expected at $\eta_c \approx 0.32$. The ϕ of the whole system is just the simple average of ϕ_s and ϕ_f, where ϕ_s is essentially zero. The Binder cumulants and the order parameter distributions show the characteristics of discontinuous transition as expected [shown in Fig. 13(d)].

Density can also be a parameter for studying this system. The results presented above are for a fixed density $\rho = 0.5$. However, at higher densities, the traveling bands may appear at lower velocities. Thus, one expects discontinuous transitions to occur for lower velocity regimes at higher densities. Such systems are computationally expensive as they involve a large number of interacting particles.

VI. CONCLUSION

A binary mixture of SPPs displays a variety of collective patterns, such as directed lanes, clusters, clumps, microclusters, microclumps, and others at different values of angular noise. The lane patterns of sSPPs at a very low angular noise are supposed to be the outcome of shear between the two species of different velocities. With a small increase in noise, the lanes formed by the slow-moving species break down into clumps, resulting in a drastic structural change in the system. Due to a large difference in velocities between the two species, finite phase segregation occurs in the system at low noise. In the steady state, the two species of the system are found to be orientationally phase synchronized irrespective of their velocities. The two-point correlation function extends throughout the system below a critical noise. At the critical noise, the system undergoes a velocity-dependent orientational order-disorder transition. The nature of the transition is found to be continuous for $v_f < 100v_s$ with $v_s = 0.01$ and discontinuous above this limit. However, the continuous transitions are nonuniversal as their critical exponents depend on the velocities. The model results depend on the density of species and the radius of interaction among the species.

ACKNOWLEDGMENT

We gratefully acknowledge the computational facilities "Newton HPC" and "Param-Ishan" provided by the Department of Physics, Indian Institute of Technology Guwahati, Assam, India.

[1] V. Schaller, C. Weber, C. Semmrich, E. Frey, and A. R. Bausch, Nature (London) **467**, 73 (2010).
[2] S. Köhler, V. Schaller, and A. R. Bausch, Nat. Mater. **10**, 462 (2011).
[3] J. D. Murray, *Mathematical Biology II: Spatial Models and Biomedical Applications* (Springer, Berlin, 2001), Vol. 3.
[4] R. Thar and M. Kühl, FEMS Microbiol. Lett. **246**, 75 (2005).
[5] A. Sokolov, I. S. Aranson, J. O. Kessler, and R. E. Goldstein, Phys. Rev. Lett. **98**, 158102 (2007).
[6] H. Zhang, A. Be'Er, R. S. Smith, E.-L. Florin, and H. L. Swinney, Europhys. Lett. **87**, 48011 (2009).
[7] H.-P. Zhang, A. Be'er, E.-L. Florin, and H. L. Swinney, Proc. Natl. Acad. Sci. USA **107**, 13626 (2010).
[8] I. D. Couzin and N. R. Franks, Proc. R. Soc. London B **270**, 139 (2003).
[9] J. Buhl, D. J. Sumpter, I. D. Couzin, J. J. Hale, E. Despland, E. Miller, and S. J. Simpson, Science **312**, 1402 (2006).
[10] P. Romanczuk, I. D. Couzin, and L. Schimansky-Geier, Phys. Rev. Lett. **102**, 010602 (2009).
[11] W. Herrnkind, Science **164**, 1425 (1969).
[12] R. G. Bill and W. F. Herrnkind, Science **193**, 1146 (1976).
[13] N. C. Makris, P. Ratilal, D. T. Symonds, S. Jagannathan, S. Lee, and R. W. Nero, Science **311**, 660 (2006).

[14] M. Ballerini, N. Cabibbo, R. Candelier, A. Cavagna, E. Cisbani, I. Giardina, V. Lecomte, A. Orlandi, G. Parisi, A. Procaccini *et al.*, Proc. Natl. Acad. Sci. USA **105**, 1232 (2008).
[15] A. Cavagna, A. Cimarelli, I. Giardina, G. Parisi, R. Santagati, F. Stefanini, and M. Viale, Proc. Natl. Acad. Sci. USA **107**, 11865 (2010).
[16] D. Helbing and P. Molnar, Phys. Rev. E **51**, 4282 (1995).
[17] Y.-Q. Jiang, B.-K. Chen, B.-H. Wang, W.-F. Wong, and B.-Y. Cao, Front. Phys. **12**, 124502 (2017).
[18] V. Narayan, S. Ramaswamy, and N. Menon, Science **317**, 105 (2007).
[19] J. Deseigne, O. Dauchot, and H. Chaté, Phys. Rev. Lett. **105**, 098001 (2010).
[20] T. Vicsek, A. Czirók, E. Ben-Jacob, I. Cohen, and O. Shochet, Phys. Rev. Lett. **75**, 1226 (1995).
[21] M. Nagy, I. Daruka, and T. Vicsek, Physica A **373**, 445 (2007).
[22] T. Vicsek and A. Zafeiris, Phys. Rep. **517**, 71 (2012).
[23] H. Chaté, F. Ginelli, G. Grégoire, and F. Raynaud, Phys. Rev. E **77**, 046113 (2008).
[24] S. Adhikary and S. B. Santra, Europhys. Lett. **135**, 48003 (2021).
[25] F. Ginelli, Eur. Phys. J. Spec. Top. **225**, 2099 (2016).
[26] S. Mishra, K. Tunstrøm, I. D. Couzin, and C. Huepe, Phys. Rev. E **86**, 011901 (2012).
[27] J. P. Singh and S. Mishra, Physica A **544**, 123530 (2020).
[28] M. E. Cates and J. Tailleur, Annu. Rev. Condens. Matter Phys. **6**, 219 (2015).
[29] C. Bechinger, R. Di Leonardo, H. Löwen, C. Reichhardt, G. Volpe, and G. Volpe, Rev. Mod. Phys. **88**, 045006 (2016).
[30] S. N. Weber, C. A. Weber, and E. Frey, Phys. Rev. Lett. **116**, 058301 (2016).
[31] S. Kumari, A. S. Nunes, N. A. Araújo, and M. M. Telo da Gama, J. Chem. Phys. **147**, 174702 (2017).
[32] J. Stenhammar, R. Wittkowski, D. Marenduzzo, and M. E. Cates, Phys. Rev. Lett. **114**, 018301 (2015).
[33] P. Dolai, A. Simha, and S. Mishra, Soft Matter **14**, 6137 (2018).
[34] R. C. Maloney and C. K. Hall, Langmuir **36**, 6378 (2020).
[35] S. R. McCandlish, A. Baskaran, and M. F. Hagan, Soft Matter **8**, 2527 (2012).
[36] A. M. Menzel, Phys. Rev. E **85**, 021912 (2012).
[37] C. Reichhardt, J. Thibault, S. Papanikolaou, and C. J. O. Reichhardt, Phys. Rev. E **98**, 022603 (2018).
[38] M. Ikeda, H. Wada, and H. Hayakawa, Europhys. Lett. **99**, 68005 (2012).
[39] N. Bain and D. Bartolo, Nat. Commun. **8**, 15969 (2017).
[40] B.-Q. Ai, Z.-G. Shao, and W.-R. Zhong, Soft Matter **14**, 4388 (2018).
[41] B. Liebchen and D. Levis, Phys. Rev. Lett. **119**, 058002 (2017).
[42] P. B. Sampat and S. Mishra, Phys. Rev. E **104**, 024130 (2021).
[43] F. D. C. Farrell, M. C. Marchetti, D. Marenduzzo, and J. Tailleur, Phys. Rev. Lett. **108**, 248101 (2012).
[44] S. B. Santra, S. Schwarzer, and H. Herrmann, Phys. Rev. E **54**, 5066 (1996).
[45] X. Yang, M. L. Manning, and M. C. Marchetti, Soft Matter **10**, 6477 (2014).
[46] M. Romenskyy and V. Lobaskin, Eur. Phys. J. B **86**, 91 (2013).
[47] K. Binder, Rep. Prog. Phys. **50**, 783 (1987).
[48] K. Christensen and N. R. Moloney, *Complexity and Criticality* (World Scientific, Singapore, 2005), Vol. 1.
[49] D. S. Cambui, A. S. de Arruda, and M. Godoy, Physica A **444**, 582 (2016).
[50] G. Baglietto and E. V. Albano, Phys. Rev. E **78**, 021125 (2008).